International Journal of Nanomedicine

Dovepress
open access to scientific and medical research

Open Access Full Text Article

ORIGINAL RESEARCH

Polydopamine-Based Nanoparticles for Synergistic Chemotherapy of Prostate Cancer

Kebang Hu[1], Dongqi Zhang[1], Weiran Ma[2], Yanzhi Gu[2], Jiang Zhao[3], Xupeng Mu[4]

[1]Department of Urology, Lequn Branch, The First Hospital of Jilin University, Changchun, 130031, People's Republic of China; [2]College of Pharmacy, Jilin University, Changchun, 130021, People's Republic of China; [3]Department of Urology, Xi'an First Hospital, Xi'an, 710002, People's Republic of China; [4]Scientific Research Center, China-Japan Union Hospital of Jilin University, Changchun, 130033, People's Republic of China

Correspondence: Jiang Zhao, Department of Urology, Xi'an First Hospital, Xi'an, 710002, People's Republic of China, Email 765398883@qq.com; Xupeng Mu, Scientific Research Center, China-Japan Union Hospital of Jilin University, Changchun, 130033, People's Republic of China, Email muxupeng@jlu.edu.cn

Introduction: Immune regulatory small molecule JQ1 can block its downstream effector PD-L1 pathway and effectively reverse the PD-L1 upregulation induced by doxorubicin (DOX). So the synergistic administration of chemotherapeutic drug DOX and JQ1 is expected to increase the sensitivity of tumors to immune checkpoint therapy and jointly enhance the body's own immunity, thus effectively killing tumor cells. Therefore, a drug delivery system loaded with DOX and JQ1 was devised in this study.

Methods: Polydopamine nanoparticles (PDA NPs) were synthesized through spontaneous polymerization. Under appropriate pH conditions, DOX and JQ1 were loaded onto the surface of PDA NPs, and the release of DOX and JQ1 were measured using UV-Vis or high performance liquid chromatography (HPLC). The mechanism of fabricated nanocomplex in vitro was investigated by cell uptake experiment, cell viability assays, apoptosis assays, and Western blot analysis. Finally, the tumor-bearing mouse model was used to evaluate the tumor-inhibiting efficacy and the biosafety in vivo.

Results: JQ1 and DOX were successfully loaded onto PDA NPs. PDA-DOX/JQ1 NPs inhibited the growth of prostate cancer cells, reduced the expression of apoptosis related proteins and induced apoptosis in vitro. The in vivo biodistribution indicated that PDA-DOX/JQ1 NPs could accumulated at the tumor sites through the EPR effect. In tumor-bearing mice, JQ1 delivered with PDA-DOX /JQ1 NPs reduced PD-L1 expression at tumor sites, generating significant tumor suppression. Furthermore, PDA-DOX/JQ1 NPs could reduce the side effects, and produce good synergistic treatment effect in vivo.

Conclusion: We have successfully prepared a multifunctional platform for synergistic prostate cancer therapy.

Keywords: prostate cancer, doxorubicin, JQ1, polydopamine, chemotherapy, PD-L1

Introduction

Prostate cancer (PCa) is the second most common malignancy in men, with an increasing incidence trend.[1,2] In clinical practice, in order to improve the cure rate, two or more methods are often used in combination for treatment. In recent years, the combination of immunotherapy and chemotherapy has become a hot topic in solid tumor research. Doxorubicin (DOX) is a well-known anticancer drug used to treat various cancers,[3,4] but DOX can also cause upregulation of PD-L1 expression in tumor cells, leading to T cell inactivation through the PD-1/PD-L1 pathway.[5,6] Meanwhile, DOX is prone to serious toxic side effects and is easily cleared by the liver or kidneys, greatly reducing the therapeutic effect on tumors.[7] Therefore, it is necessary to develop more effective nano delivery systems to improve the tumor delivery efficiency of DOX and reduce its toxic side effects. JQ1 is a small molecule inhibitor of bromodomain and extra-terminal (BET) protein BRD4, which overcomes immune tolerance by inhibiting intratumoral expression of PD-L1.[8] The BET inhibitor JQ1 can reduce PD-L1 expression on tumor cells, tumor-associated dendritic cells, and macrophages, thereby increasing the activity of anti-tumor cytotoxic T cells.[8–10] Moreover, the BET inhibitors can inhibit the macrophage inflammatory response and attenuate the systemic inflammatory processes without eliminating the antitumor immune response.[11,12] JQ1 can also block the transcription of c-Myc and suppress tumor glycolysis.[13]

Received: 14 March 2024
Accepted: 27 June 2024
Published: 3 July 2024

Graphical Abstract

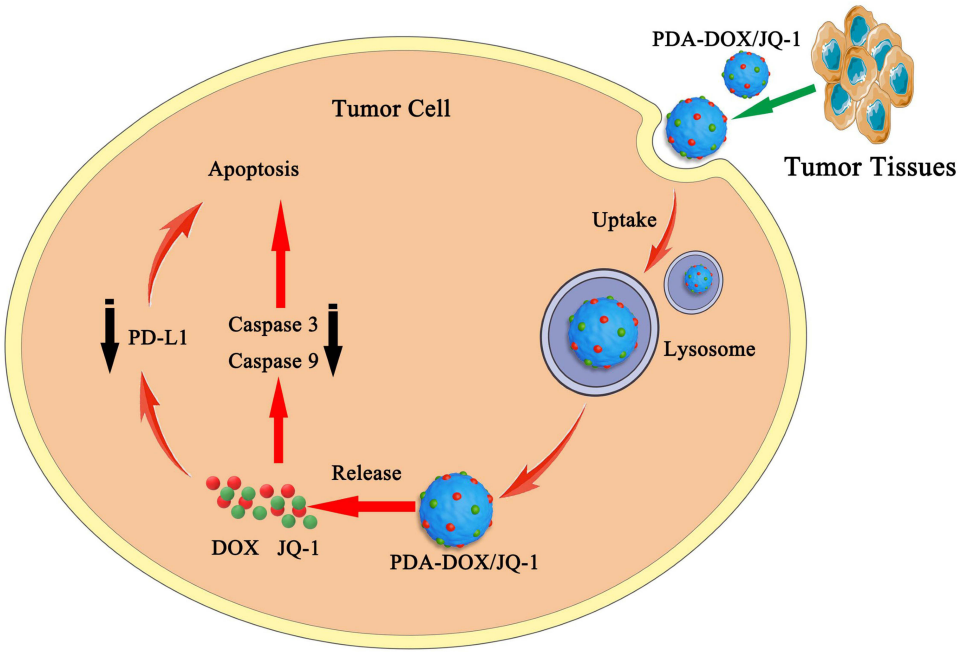

However, its single use may not produce sufficient therapeutic effects, so it is often used in combination with other drugs.[14–16] Since DOX treatment can lead to increased expression of PD-L1 on tumor cells, thus limiting tumor immunotherapy. JQ1 is used as an inhibitor of BET and can block its downstream effector PD-L1 pathway, which means JQ1 can effectively reverse the PD-L1 upregulation induced by DOX. Therefore, the synergistic administration of DOX and immune regulatory small molecule JQ1 is expected to enhance the sensitivity of tumors to immune checkpoint therapy, thereby effectively killing tumor cells. Nanotechnology, due to its various excellent characteristics, provides a new method to solve the problems of traditional chemotherapy in synergistic anti-tumor therapy. So far, some nanocarriers have been prepared to deliver DOX and JQ1 for tumor treatment.[17–19] Liu et al engineered a charge reversal yolk-shell liposome co-loaded with DOX and JQ1 to treat melanoma, which could enhance tumor chemotherapy via blockade of the PD-L1 pathway.[17] Gu et al developed a DOX and JQ1 loaded pH-responsive hydrogel (DOX-JQ1@Gel) for combinatorial chemoimmunotherapy tailored to the tumor microenvironment. The DOX-JQ1@Gel could treat breast tumors with poor responses to ICB after intratumor injection.[18] Zhao et al developed a ROS-responsive hyaluronan-modified polydopamine nanoarray (DOX/JQ1-IBRN) for delivering DOX/JQ1. The local implantation of DOX/JQ1-IBRN achieved suppression of recurrent melanoma and breast tumors, and significantly prolonged the period of survival.[19] However, there is no relevant research on the synergistic effect of DOX and JQ1 in PCa.

PCa with local progression or distant metastasis is mainly treated with chemotherapy drugs. However, chemotherapy drugs have drawbacks, such as low bioavailability. Therefore, higher doses of medication must be administered to achieve therapeutic effects, but this can make adverse side effects more pronounced.[20] There is an urgent need for a more effective approach to improve treatment effectiveness and reduce adverse side effects.[21,22] Nanocarriers have excellent drug loading and sustained-release properties, better efficacy and safety, providing new solutions for the development of cancer treatment.[23,24] Polydopamine nanoparticles (PDA NPs) are melanin polymers produced by oxidative self polymerization of dopamine under certain conditions.[25] PDA NPs have good biocompatibility, are very easy to synthesize and modify, have negligible cytotoxicity, and can alleviate inflammatory reactions. These characteristics of PDA NPs make it suitable for widespread use as a drug carrier in the biomedical field.[26,27] In this study, we utilized the advantages of PDA NPs to successfully construct a drug delivery system loaded with DOX and JQ1 (PDA-DOX/JQ1) for the synergistic

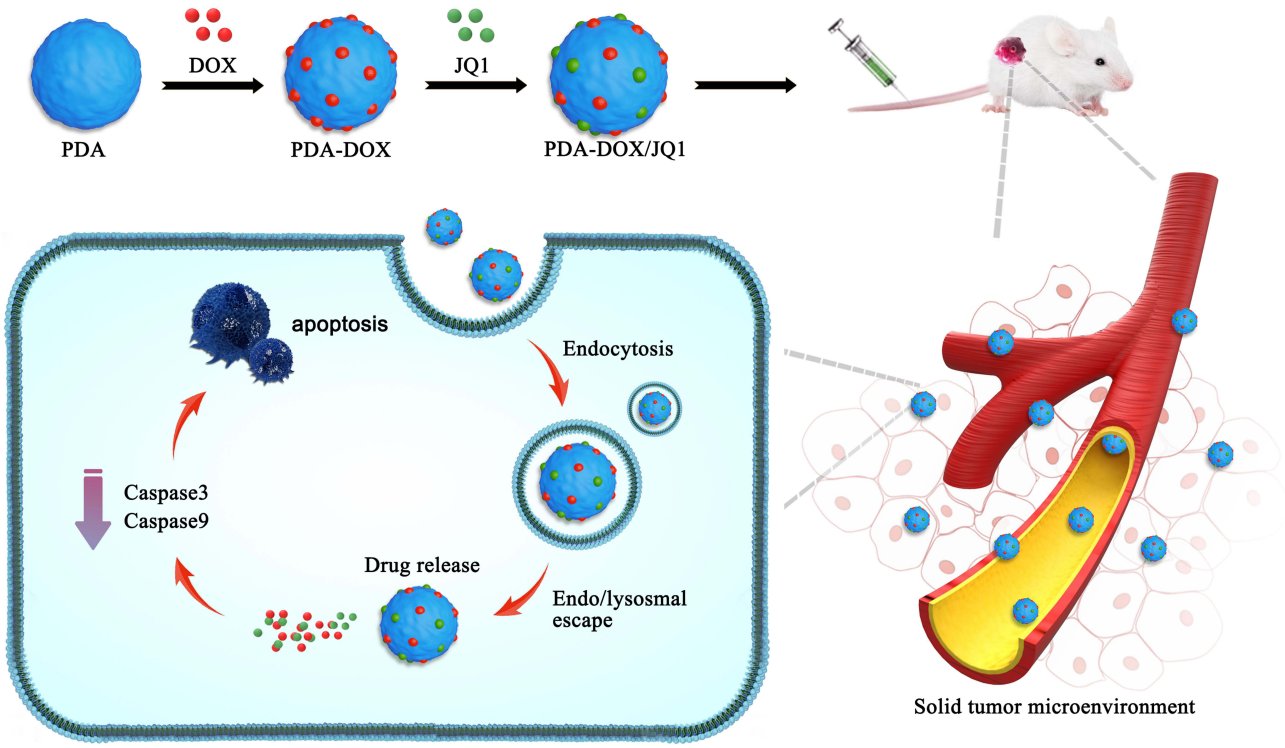

Figure 1 Schematic of the preparation of PDA-DOX/JQ1 NPs and the combination therapy for PCa in vivo.

treatment of PCa. In tumor targeted drug delivery, the enhanced permeation and retention (EPR) effect of macromolecules is a key mechanism for achieving solid tumor targeting.[28–30] So the PDA-DOX/JQ1 NPs administrated through systemic injection accumulated in tumor tissue through the EPR effect to regress tumor growth. Furthermore, PDA-DOX /JQ1 NPs could reduce the side effects, and produce good synergistic treatment effect in vivo (Figure 1).

Materials and Methods

Materials and Reagents

Ham's F-12K and penicillin-streptomycin were purchased from Procell (China). TUNEL apoptosis assay kit, Cell counting kit-8 (CCK-8), and BCA protein assay kit were obtained from Beyotime (China). Dopamine hydrochloride, JQ-1, and Doxorubicin hydrochloride (DOX) were bought from MedChemExpress (NJ, USA). Other laboratory biochemical reagents were purchased from Solarbio (China). The antibodies including PD-L1, Caspase-3, Caspase-9, Bax, and β-actin were obtained from Proteintech (IL, USA).

Cells Culture

Human prostate cancer cells PC-3 were obtained from Procell (China). PC-3 cells were cultured in Ham's F-12K medium supplemented with 10% FBS and 1% penicillin-streptomycin. The cells were incubated in a 5% CO_2 incubator at 37 °C.

Preparation and Characterization of PDA NPs

PDA NPs were synthesized based on the previous reports.[31] Firstly, 10 mL anhydrous ethanol was added to 50 mL Tris solution (10 mM) and magnetically stirred for 10 min at room temperature. Then, 25 mg Dopamine hydrochloride was dissolved in 2.5 mL of ultrapure water to a final concentration of 10 mg/mL and slowly added to the above mixture solution. After stirring at room temperature for 16 h, the color of the solution changed from colorless to brown and gradually deepened to black. Finally, the solution was centrifuged and washed with deionized water. The precipitate obtained was PDA NPs. Transmission electron microscopy (TEM) (Jeol, Akishima Tokyo, Japan) was used to

characterize the particle size and morphology of PDA NPs. The hydrodynamic diameter was measured by dynamic light scattering (DLS) using a Zetasizer Nano-ZS instrument (Malvern Instruments, Malvern, UK).

Drug Loading

PDA NPs (1mg/mL, 0.5mL) was suspended in 10×Tris-buffer and mixed with 1 mL, 0.5 mL, 0.25 mL, 0.125 mL, 0.0625 mL DOX solution (1mg/mL), respectively. After stirring at room temperature for 24 h, the solution was centrifuged and washed with deionized water. The obtained precipitate was PDA NPs loaded with DOX (PDA-DOX NPs). The supernatants were collected after centrifugation separately, and the absorbance at 480 nm was determined using a UV-visible spectrometer. The concentration of unloaded DOX in the supernatant was calculated according to the standard curve. The loading efficiency of DOX was calculated as follows: LE(%) = (weight of loaded DOX/weight of PDA+ weight of loaded DOX)×100%.[26]

PDA NPs (1mg/mL) was suspended in 10×Tris-buffer, and then mixed with JQ1 solution(1mg/mL). After incubating at room temperature for 24 h, the solution was centrifuged for 15min (12000 r/min) and the resulting precipitate was PDA NPs loaded with JQ1 (PDA-JQ1 NPs). The absorbance of the supernatants at 255 nm was determined using a UV-visible spectrometer.

The fabrication of PDA-DOX/JQ1 NPs was similar to described above. PDA-DOX NPs obtained from PDA NPs (0.5mg) and DOX (0.5mg) were mixed with different concentrations of JQ1 (1mg/mL; 0.25 mL, 0.5 mL, and 1 mL). After incubating for 24 h without light, PDA-DOX/JQ1 NPs were obtained by centrifugation. The supernatant was collected after centrifugation and the loading of JQ1 was determined by a HPLC. The HPLC system consisted of a reverse-phase C-18 column (Symmetry), with a mobile phase of acetonitrile and water (80:20 v/v) pumped at a flow rate of 1.0 mL/min at 25 °C. The column effluent was detected at 255 nm by a UV detector.

In vitro DOX Release

The prepared PDA-DOX or PDA-DOX/JQ1 was dissolved in PBS solution at pH 5.0 or pH 7.0 with moderate shaking for different periods of time. At desired time point (1, 2, 6, 12, 24, 48 h), the supernatant was collected and the amount of DOX released was measured by the UV-visible spectrometer.

Cell Proliferation Assays

The CCK-8 assay was used to assess the inhibitory effect of PDA-DOX/JQ1 NPs on tumor cells in vitro. 1×10^4 PC-3 cells were seeded in 96-well plates and then co-incubated with different formulation for 24 h. The experimental groups included DOX, PDA-DOX, PDA-JQ1, PDA-DOX+PDA-JQ1, and PDA-DOX/JQ1. After incubation, CCK-8 solution (10 μL) was added to each well for 1 h without light. The absorbance at 450 nm was measured using a microplate reader (ELx-800, BioTek Instruments, USA), and the cell viability was calculated.

In vitro Cellular Uptake

PC-3 cells (2×10^4 cells/well) were seeded in the 6-well plates. After 24 h, cells were incubated with DOX or PDA-DOX for 4 h and then fixed with 4% paraformaldehyde for 15 min. Thereafter, the cells were washed with PBS and stained with DAPI. The stained cells were observed under a fluorescence microscope (IX83, Olympus, Japan).

Apoptosis Assay

PC-3 cells (2×10^5 cells/well) were treated with free DOX, PDA-DOX, PDA-DOX+PDA-JQ1, PDA-DOX/JQ1 NPs for 24 h, respectively. After incubation, the cells were treated with Annexin V-FITC/PI according to the instructions to quantitatively analyze cell apoptosis. All samples were analyzed by Cytomics™ FC 500 flow cytometer (Beckman, USA) within 1 h.

Western Blot Analysis

PC-3 cells (2×10^5 cells/well) were seeded in 6-well plates and incubated with different formulation for 24 h. Then, proteins were extracted using RIPA lysis (Beyotime, China), and the protein concentrations were determined using BCA

protein assay kit (Beyotime, China). Subsequently, the protein samples were loaded on 10% SDS-PAGE and transferred to a Nitrocellulose membrane. After blocking with 5% skimmed milk, the membranes were incubated with the primary anti-PD-L1, Caspase-3, Caspase-9, Bax, or anti-β-actin antibodies overnight at 4 °C, respectively. After washing with TBST buffer, the membranes were further incubated with specific secondary antibodies for 1.5 h. The results were analyzed by an Odyssey infrared imaging system (LI-COR Biosciences, NE, USA).

Biosafety and Biodistribution in vivo

Male BALB/c nude mice (4–6 weeks old) were purchased from Vital River Company (Beijing, China) and housed under specific pathogen-free conditions. PC-3 cells (5×10^6) were suspended in 100 uL PBS and subcutaneously inoculated into the right side of the mice. When the PC-3 xenograft tumor reached about 100 mm^3, PBS, DOX, PDA-DOX NPs NPs (100 μL, DOX: 5 mg/kg) were injected through the tail vein. After 24 h, the mice were euthanized. Then, major organs and tumors were collected, weighed, and homogenized in lysis buffer. Subsequently, the lysate of each sample was centrifuged and fluorescence intensity of DOX in the supernatant was measured at 480 nm with a microplate reader (Bio-Rad, CA, USA). Meanwhile, the blood samples were collected for complete blood panel tests by an automatic biochemical analyzer.

The tumor-bearing mice were further intravenously injected with cy5.5 labeled PDA (PDA-cy5.5). After injection, mice were anesthetized, and the fluorescent intensity was observed via the In Vivo Imaging System (PerkinElmer, USA) at 4 h, 8h, 24 h, and 48 h, respectively. Finally, mice were sacrificed at 48 h post-injection, tumor tissues and the main organs including heart, liver, spleen, lung, and kidneys were collected for ex vivo fluorescence imaging.

Anticancer Efficacy in vivo

When the PC-3 xenograft tumor reached about 100 mm^3, mice were randomly divided into 5 groups which were treated with PBS, free DOX, PDA-DOX, PDA-DOX+PDA-JQ1, and PDA-DOX/JQ1 NPs (DOX dose: 5 mg/kg) through the tail vein 7 times at an interval of 2 days, respectively. The tumor volume and body weight were measured every 2 days. The tumor volume (V) was calculated using the formula: $V=0.5\times length\times width^2$. All mice were euthanized 14 days after administration, the major organs and tumor tissues were collected and sectioned for histological examination by hematoxylin and eosin (H&E) staining or immunohistochemical staining.

Statistical Analysis

All experimental data were expressed as mean value ± SD. Statistical analysis were determined by one-way analysis of variance. $P < 0.05$ was considered significant.

Results and Discussion

Preparation and Characterization of PDA-DOX/JQ1 NPs

PDA NPs were synthesized based on the principle that dopamine could oxidize and self polymerize in weakly alkaline solutions. The synthesized PDA NPs was brownish black in color. The TEM image showed that the mean size of as-prepared PDA NPs was approximately 95 nm (Figure 2A). Given that PDA has a large number of surface functional groups, such as catechol and amino groups, DOX and JQ1 could bind to the outer surface of PDA NPs via π-π conjugation and hydrogen bonding interactions. PDA NPs were mixed with different amounts of DOX in Tris-buffer (pH 8.0) overnight. As shown in Figure 2B, the UV-vis absorption spectrum of PDA-DOX demonstrated significant absorption near the wavelength of 480 nm compared to PDA, confirming the successful loading of DOX by PDA NPs. With the increase of DOX concentration, the DOX loading amount of PDA NPs gradually increased. Due to the impact of excessive loading on the stability of PDA NPs, the PDA-DOX obtained from DOX (1 mg/mL, 0.5 mL) was selected for the next step of the experiment. Under these conditions, the average DOX loading amount of PDA NPs was 365 ± 10 μg. The drug loading rate was about 42% (Figure 2C).

Meanwhile, as shown in Figure 2D, after mixing PDA (1mg) with different concentrations of JQ1, the UV-vis absorption spectrum of PDA-JQ1 exhibited an absorption peak near 255 nm that was similar to JQ1, confirming the

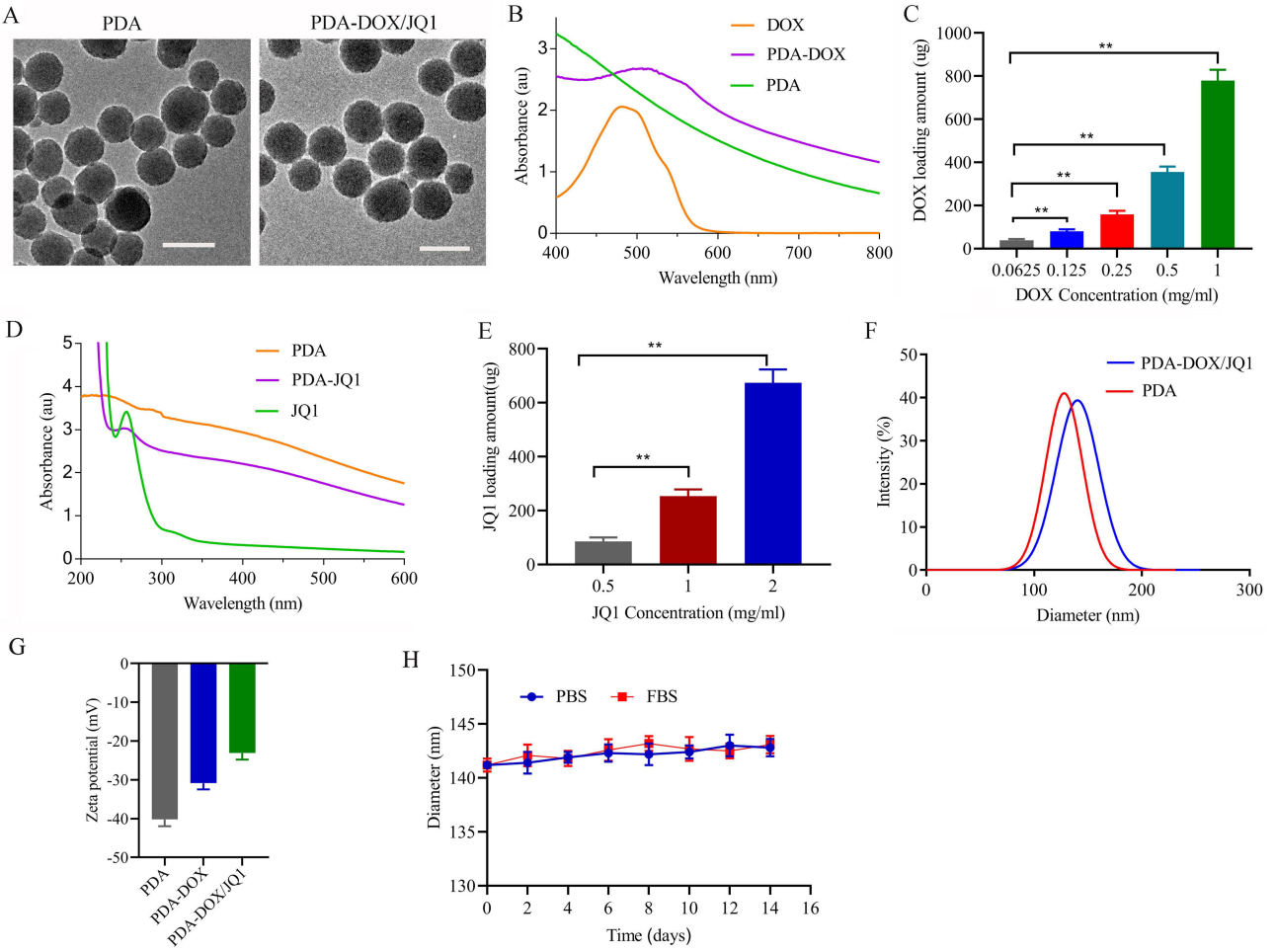

Figure 2 Preparation and characterization of PDA-DOX/JQ1 NPs. (**A**) TEM images of PDA NPs and PDA-DOX/JQ1 NPs. Scale bar = 100 nm. (**B**) The UV-vis absorbance spectra of DOX, PDA NPs, and PDA-DOX NPs. (**C**) The DOX loading amount of PDA NPs under various proportions (DOX:PDA). (**D**) The UV-vis absorbance spectra of JQ1, PDA NPs, and PDA-JQ1 NPs. (**E**) The JQ1 loading amount of PDA-DOX NPs. (**F**) Hydrodynamic diameters of PDA NPs and PDA-DOX/JQ1 NPs. (**G**) Surface zeta potential of different formulations. (**H**) Stability of PDA-DOX/JQ1 NPs by measurement of particle size. $^{**}p < 0.01$.

successful JQ1 loading by PDA NPs. Finally, the PDA-DOX/JQ1 NPs were synthesized. PDA-DOX NPs obtained from PDA NPs (0.5mg) and DOX (0.5mg) were mixed with different concentrations of JQ1 (1mg/mL; 0.25 mL, 0.5 mL, and 1 mL) overnight. The loading of JQ1 was determined by a HPLC. With the increase of JQ1 concentration, the JQ1 loading amount of PDA NPs also gradually increased (Figure 2E). The average loading amount of JQ1 (1mg/mL; 0.5 mL) in PDA-DOX/JQ1 NPs was 140 ± 2 μg. The drug loading rate was about 14%. The small-molecule JQ1 and DOX loaded onto PDA NPs via π–π conjugation did not significantly change its size from the PDA-DOX/JQ1 TEM (Figure 2A). Meanwhile, dynamic light scattering (DLS) analysis confirmed the successful loading of JQ1 and DOX as the hydrodynamic diameter of PDA NPs increased from 126 ± 10.2 nm to 141 ± 9.8 nm (Figure 2F). Meanwhile, the surface zeta potential values of PDA NPs shifted from −40.2 mV to −23.1 mV after JQ1 and DOX loading (PDA-DOX /JQ1) (Figure 2G). We then checked the stability of PDA-DOX/JQ1 NPs. PDA-DOX/JQ1 NPs (1 mg/mL) were suspended in PBS and FBS for 14 days and the particle size was monitored. The change in particle size of PDA-DOX /JQ1 NPs was almost negligible (Figure 2H). Taken together, these results suggested that JQ1 and DOX were successfully loaded onto PDA NPs.

Drug Release in vitro

The drug release profiles of as-prepared PDA-DOX/JQ1 NPs were evaluated. As shown in Figure 3A, the cumulative release ratio of DOX was slow at pH 7.4 within 48 h. However, the DOX release rate and amount were significantly

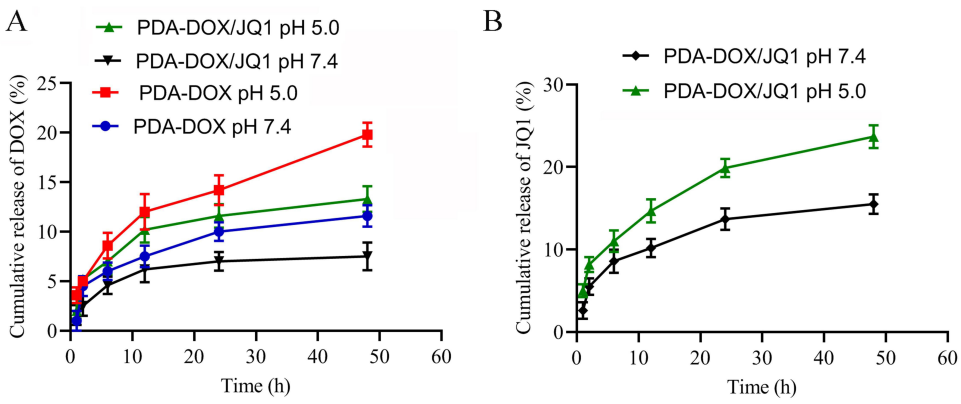

Figure 3 Drug-releasing capacity of PDA-DOX/JQ1 NPs. (**A**) Release profile of DOX from PDA-DOX NPs and PDA-DOX/JQ1 NPs at different pH within 48 h. (**B**) JQ1 release from PDA-DOX/JQ1 NPs at different pH within 48 h.

increased under acidic conditions (pH 5.0). Within 48 h, PDA-DOX NPs released ~19.8% of DOX at pH 5.0, and 11.6% at pH 7.4. In PDA-DOX/JQ1, both DOX and JQ1 need to be released simultaneously, and there is a competitive relationship between DOX and JQ1. Furthermore, the π-π stacking interactions between DOX and JQ1 also affects its release. So, the release rate of DOX in PDA-DOX/JQ1 was slower than that in PDA-DOX due to the addition of JQ1. Under the same conditions, the release of DOX in PDA-DOX/JQ1 was only about 13.3% (Figure 3A). By comparison, approximately 23% of JQ1 was released from PDA-DOX/JQ1 NPs at pH 5.0 within 48 h (Figure 3B).

Efficacy of PDA-DOX NPs in Targeting Tumor Cells

To assess the targeting ability of the prepared PDA-DOX/JQ1 NPs in vitro, free DOX, or PDA-DOX NPs were incubated with PC-3 cells for 4 h, respectively. Compared to free DOX, PC-3 cells treated with PDA-DOX NPs demonstrated higher fluorescence intensity within 4 h (Figure 4A). Meanwhile, flow cytometry analysis was used to quantitatively detect the cellular uptake and drug release in PC-3 cells. As time went on, the uptake rates of free DOX and PDA-DOX NPs by PC-3 cells gradually increased. In particular, after incubation for 6 h, the cellular uptake efficiency of DOX was as high as 88.2% for PDA-DOX NPs, about 1.5 times that of free DOX (58.3%) (Figure 4B). The results indicated that PDA-DOX/JQ1 NPs could be used for targeted delivery of anticancer drugs. We further tested the expression of PD-L1 protein in PC-3 cells after various nanomaterials treatments. As shown in Figure 4C and D, the expression of PD-L1 increased after PDA-DOX treatment. It was reported that JQ1 was able to inhibit the expression of PD-L1 because PD-L1 was a downstream effector of JQ1.[10] So low expression of PD-L1 was found in PDA-DOX/JQ1 treated cells. This indicated that PDA-DOX/JQ1 could effectively reverse the up-regulation of PD-L1 induced by DOX. The results further suggested that DOX and JQ1 might produce synergistic antitumor effects in vitro.

Combined Antitumor Therapeutic Efficacy in vitro

We further measured the effect of PDA-DOX/JQ1 on cell survival using the CCK8 assay. PC-3 cells were treated with PDA-DOX/JQ1 of different DOX concentrations or JQ1 concentrations for 24 h, respectively. As shown in Figure 5A, all groups displayed a dose-dependent cytotoxicity to PC-3 cells within 24 h. Under the same concentration, compared to PDA-JQ1 and PDA-DOX, PDA-DOX/JQ1 NPs exhibited better anti-tumor ability, which was associated with the synergistic antitumor effect (Figure 5A). In addition, we applied flow cytometry to detect cell apoptosis induced by the as-prepared nanomaterials. Compared with DOX-treated cells (12.81%), PDA-DOX/JQ1-treated cells showed a significantly higher proportion of apoptosis (35.48%) (Figure 5B and C). To further investigate the apoptosis mechanism in PC-3 cells, we examined the protein levels of Bax, cleaved caspase-3, cleaved caspase-9. Compared to the control group, PDA-DOX/JQ1 treatment significantly up-regulated the levels of Bax, cleaved caspase-3, and cleaved caspase-9 proteins, while down-regulating the level of caspase-3, and caspase-9 proteins (Figure 5D). These results

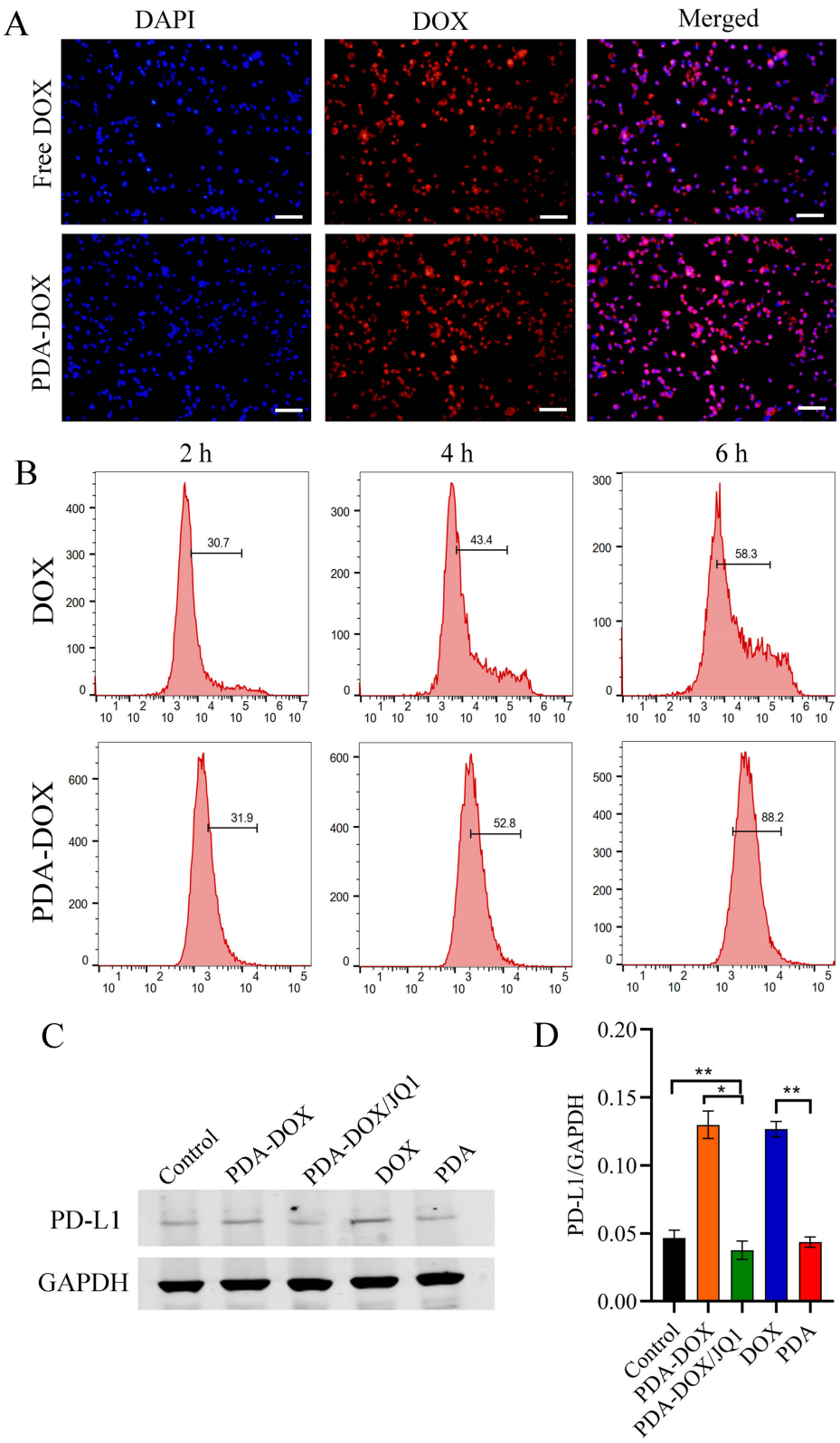

Figure 4 Efficacy of PDA-DOX NPs in targeting tumor cells. (**A**) Cellular uptake of free DOX and PDA-DOX/JQ1 NPs at 4 h analyzed by fluorescence microscope. Scale bars: 100 μm. (**B**) Cell uptake efficiency of free DOX and PDA-DOX/JQ1 NPs analyzed by flow cytometry over time (2, 4, 6 h). (**C**) Western blot analysis of PD-L1 expression in PC-3 cells after incubation with PDA, free DOX, PDA-DOX or PDA-DOX/JQ1 NPs. (**D**) Semi-quantitative analysis of the relative levels of PD-L1 in the Western blot as shown in panel (**C**). *$p < 0.05$, **$p < 0.01$.

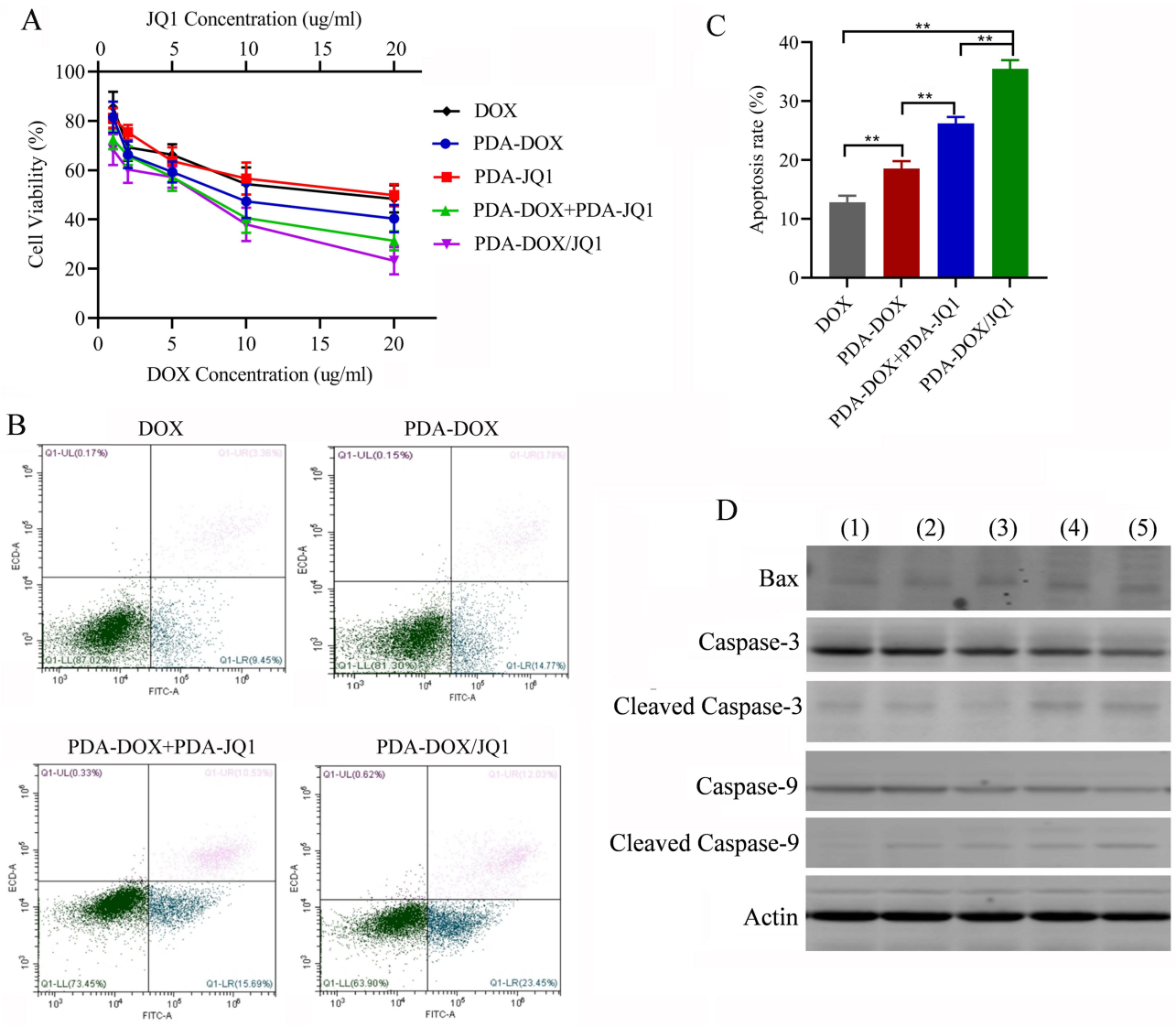

Figure 5 Combined antitumor therapeutic efficacy in vitro. (**A**) Relative cell viability of PC-3 cells after incubation with different formulations at the same concentration gradient. (**B** and **C**) Apoptosis analysis of PC-3 cells after incubation with DOX, PDA-DOX, PDA-DOX+PDA-JQ1 NPs, and PDA-DOX/JQ1 NPs. (**D**) Western blot analysis of the expression of apoptosis related proteins. (1) Control; (2) DOX; (3) PDA-DOX; (4) PDA-DOX+PDA-JQ1 NPs; and (5) PDA-DOX/JQ1 NPs. $^{**}p < 0.01$.

suggested that PDA-DOX/JQ1 could enhance cytotoxic effects in vitro and induce tumor cell apoptosis by caspase-mediated signaling pathway.

Biosafety and Biodistribution Study in vivo

Firstly, the biosafety of PDA-DOX/JQ1 in vivo was investigated. The routine blood biochemistry parameters, including hemolysis ratio, cardiac function markers (CK), renal function markers (UREA), hepatic function markers (ALT, AST) in mice treated with PDA-DOX/JQ1 were essentially similar to those of the mice treated with PBS 24 h after injection (Figure 6A). We then examined the biodistribution of PDA-DOX/JQ1 NPs in tumor-bearing nude mice which were injected with DOX or PDA-DOX/JQ1 NPs via the tail vein. The major organs and tumors were harvested 24 h after injection. In addition, compared with the DOX treatment group, PDA-DOX/JQ1 treatment exhibited less DOX accumulation in the liver and heart, indicating that PDA-DOX NPs could reduce organ phagocytosis and thus reduce cardiac toxicity of DOX (Figure 6B). Next, the tumor-targeting ability of PDA NPs in tumor-bearing mice were detected. Research has found that EPR effects are commonly observed in most solid tumors. And the EPR effects will allow most macromolecules or micelles

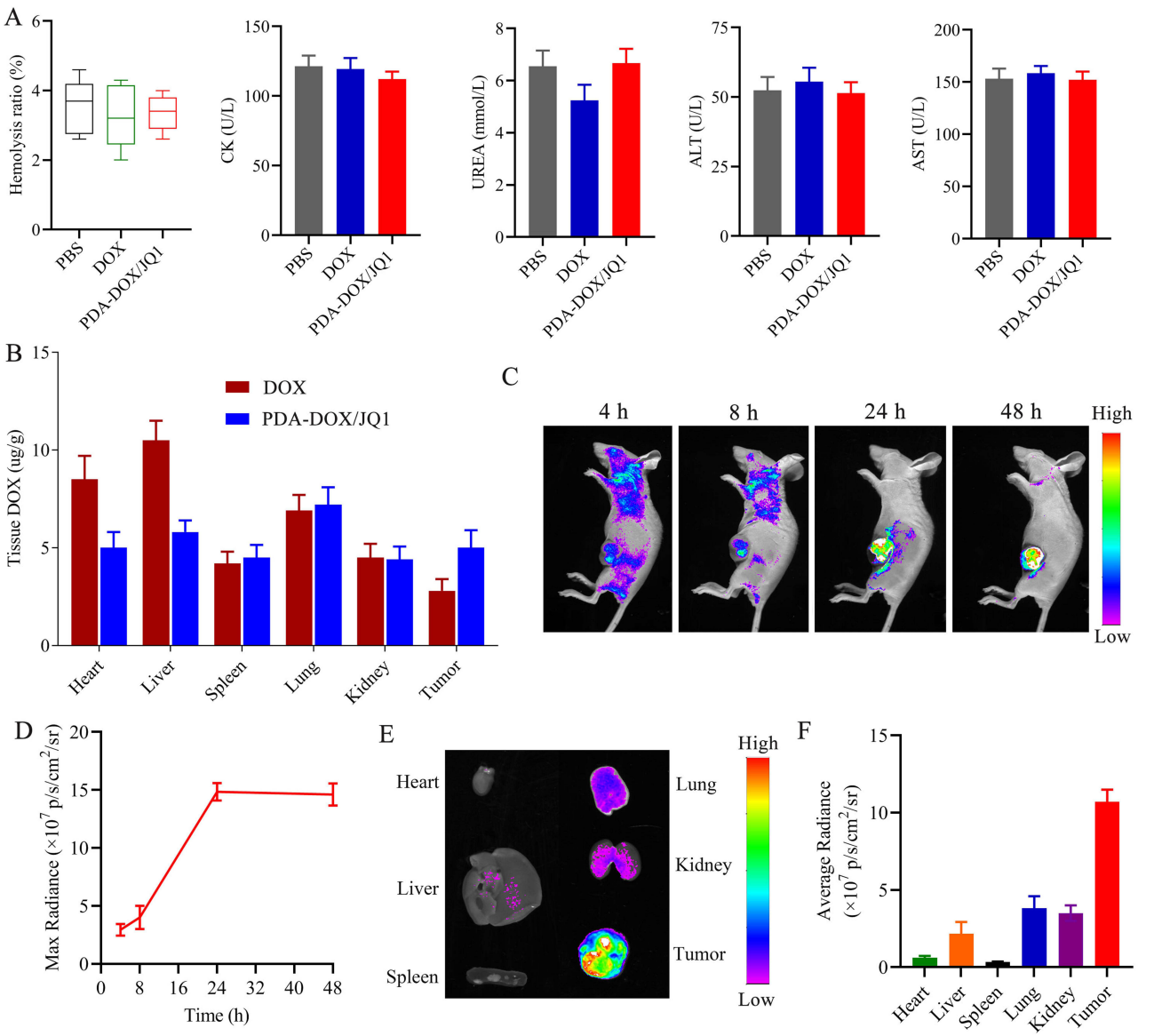

Figure 6 In vivo biosafety and biodistribution of PDA-DOX/JQ1 NPs. (**A**) Blood analysis of hemolysis ratio, CK, UREA, ALT, and AST after treatment with different formulations. (**B**) The biodistribution of DOX in tumor-bearing mice at 24 h after injection of different formulations. (**C**) In vivo fluorescence imaging of tumor-bearing mice following intravenous injection of PDA-cy5.5. (**D**) Corresponding mean fluorescence intensity of cy5.5 in the tumor areas. (**E**) Cy5 fluorescence images of major organs and tumor tissue taken from tumor-bearing mice 48 h post injection of PDA-cy5.5. (**F**) The corresponding mean fluorescence intensity analysis of the major organs quantified from the ex vivo imaging results.

to selectively target tumors and stay in tumor tissue for a long period of time.[28,29] The results showed that the fluorescence signal of cy5.5 could be detected at the tumor site of mice 4 h after injection of PDA-cy5.5. With time, the fluorescence intensity at the tumor site gradually increased due to the EPR effect. And the fluorescence signal intensity remained high even after 48 h (Figure 6C and D). Then the mice were euthanized, and the fluorescence intensity of tumor tissues and the main organs were detected at 48 h in vitro. The results showed that, except for the tumor site, PDA-cy5.5 mainly exhibited strong fluorescence intensity in the kidney and lung tissues. The quantitative average fluorescence intensity of the tumors tissues were significantly higher than that of the main organs (Figure 6E and F).

In vivo Antitumor Efficacy

Subsequently, the therapeutic efficiency of PDA-DOX/JQ1 NPs in vivo was investigated. Tumor-bearing mice were subjected to different treatments via the tail vein every 2 days as depicted in Figure 7A. The body weights of the tumor-

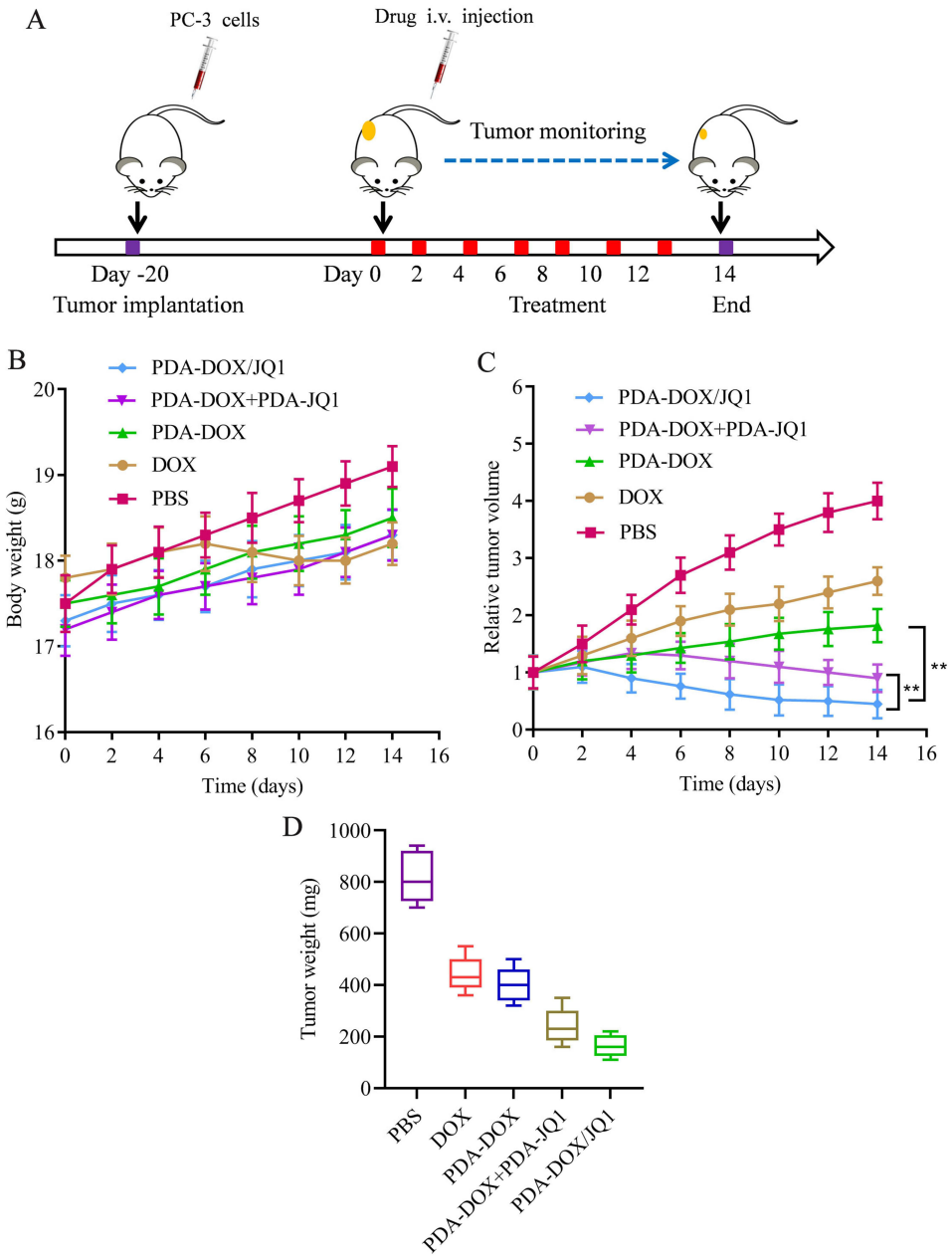

Figure 7 In vivo antitumor efficacy of PDA-DOX/JQ1 NPs. (**A**) Schematic illustration of the establishment and experimental protocol in tumor-bearing mice. (**B**) Tumor weight of each group after treatment. (**C**) Tumor growth curves of different groups after treatment. (**D**) Tumor weights of tumor-bearing mice with different treatments after 14 days. $^{**}p < 0.01$.

bearing mice in the various groups did not exhibit significant weight loss, except for the free DOX group, which displayed a slight decrease of body weight during treatment, likely due to possible side effects and acute toxicity caused by DOX (Figure 7B). Mice treated with PDA-DOX showed significant tumor inhibition compared to the control group. Notably, treatment with PDA-DOX/JQ1 NPs displayed the most pronounced tumor suppression, as evidenced by the smallest tumor volume and lowest tumor weight (Figure 7C and D). These results demonstrated that PDA-DOX/JQ1 NPs effectively delivered chemotherapeutics to the tumor sites without causing obvious systemic toxicity.

The therapeutic effects and biosafety of PDA-DOX/JQ1 NPs were further investigated by pathological examination. The immunohistochemical results revealed that compared to other groups, the PDA-DOX/JQ1 treatment group inhibited the expression of PD-L1 in tumor tissues. Ki67 staining of tumor sections was performed to assess tumor cell proliferation after

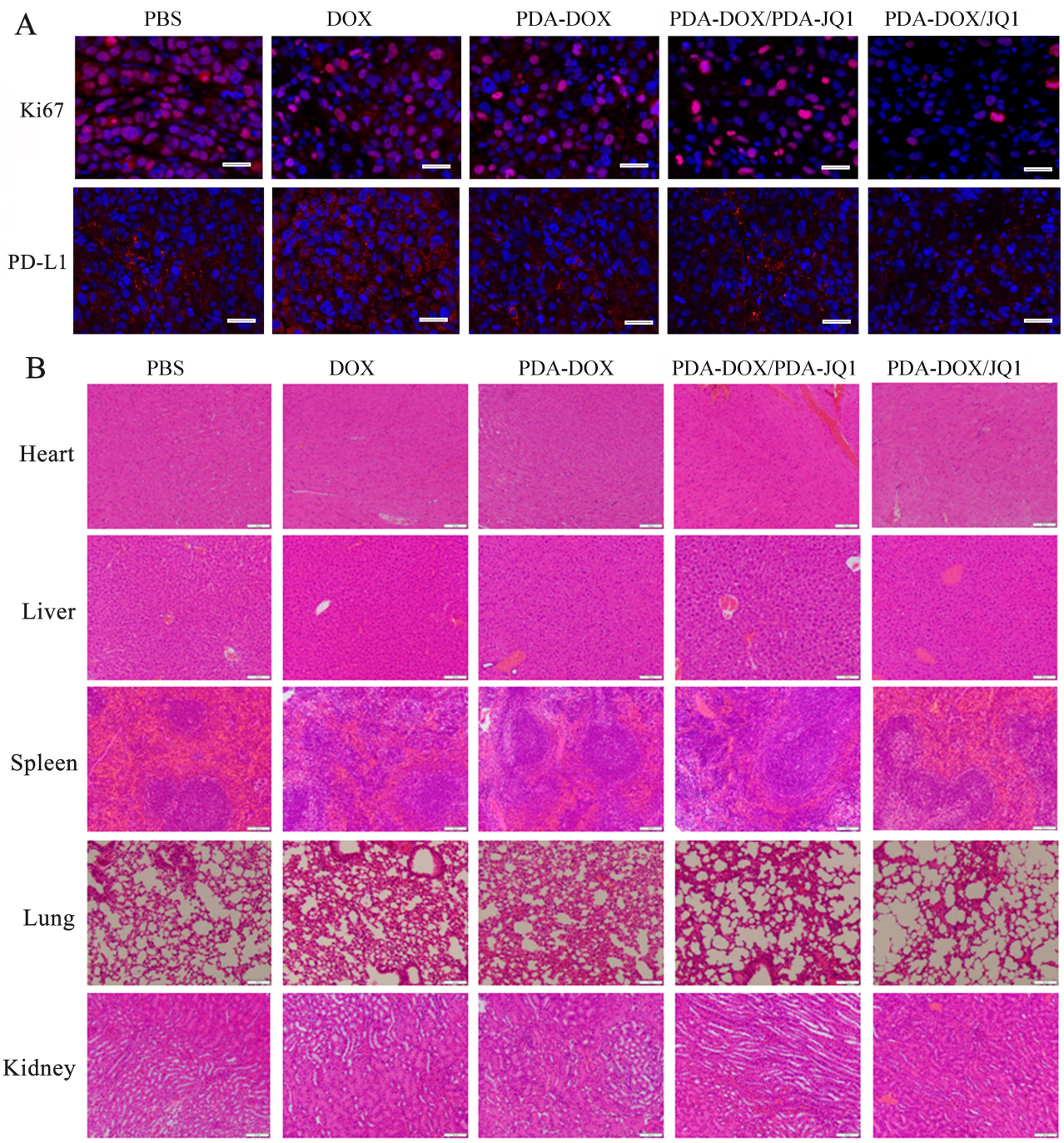

Figure 8 The evaluation of systemic toxicity through pathology. (**A**) The expression of Ki67 and PD-L1 in tumor tissues of different treatment groups. Scale bars: 50 μm. (**B**) Representative H&E staining images of major organs in the different treatment groups. Scale bars: 100μm.

different treatments. PDA-DOX/JQ1 treatment reduced the expression of cell proliferation Ki67 protein in the tumors, confirming the superior therapeutic effect of PDA-DOX/JQ1 NPs (Figure 8A). In addition, no obvious pathological changes were found in the major organs in the PDA-DOX/JQ1 group, further indicated the safety of PDA-DOX/JQ1 NPs (Figure 8B).

Conclusions

In summary, we have successfully prepared a biomimetic drug delivery system containing chemotherapeutic drug DOX and a PD-L1 suppressor JQ1 for synergistic PCa therapy. This new composite material not only had pH sensitive drug

release ability, but also could enhance the anti-tumor effect of nanodrugs. The nanodrug carriers solved the low water solubility of JQ1 and reduced the toxic side effects of DOX. Meanwhile, the PDA-DOX/JQ1 NPs could induce the apoptosis of tumor cells in vitro. In addition, the in vivo biodistribution indicated that PDA-DOX/JQ1 NPs could target and accumulate at the tumor sites. In tumor-bearing mice, JQ1 delivered with PDA-DOX/JQ1 NPs reduced PD-L1 expression at tumor sites, generating significant tumor suppression. These results demonstrated the potential of the prodrug PDA-DOX/JQ1 NPs to improve cancer immunotherapy by addressing DOX-induced up-regulation of PD-L1. We hope that the collaborative drug delivery strategy can provide more effective and convenient treatment for PCa.

Abbreviations

PCa, prostate cancer; DOX, doxorubicin; BET, bromodomain and extra-terminal; PDA, polydopamine; NPs, nanoparticles; CCK-8, cell counting kit-8; H&E, hematoxylin and eosin; TEM, transmission electron microscopy; DLS, dynamic light scattering; EPR, enhanced permeability and retention.

Ethics Statements

All animal experimental procedures were conducted in accordance with Guidelines for the Ethical Review of Laboratory Animal Welfare (GB/T 35892-2018) and approved by the Animal Welfare and Research Ethics Committee of Jilin University (Changchun, China).

Acknowledgments

This work was financially supported by the Science and Technology Development Plan Projects of Jilin Province (Grant No. 20210101272JC).

Disclosure

The authors report no conflicts of interest in this work.

References

1. Berish RB, Ali AN, Telmer PG, et al. Translational models of prostate cancer bone metastasis. *Nat Rev Urol*. 2018;15(7):403–421. doi:10.1038/s41585-018-0020-2
2. Wang Y, Wu N, Jiang N. Autophagy provides a conceptual therapeutic framework for bone metastasis from prostate cancer. *Cell Death Dis*. 2021;12(10):909. doi:10.1038/s41419-021-04181-x
3. Li R, Liu C, Wan C, et al. A targeted and pH-responsive nano-graphene oxide nanoparticle loaded with doxorubicin for synergetic chemo-photothermal therapy of oral squamous cell carcinoma. *Int J Nanomedicine*. 2023;18:3309–3324. doi:10.2147/IJN.S402249
4. D'Angelo NA, Noronha MA, Câmara MCC, et al. Doxorubicin nanoformulations on therapy against cancer: an overview from the last 10 years. *Biomater Adv*. 2022;133:112623. doi:10.1016/j.msec.2021.112623
5. Qiu N, Liu Y, Liu Q, et al. Celastrol nanoemulsion induces immunogenicity and downregulates PD-L1 to boost abscopal effect in melanoma therapy. *Biomaterials*. 2021;269:120604. doi:10.1016/j.biomaterials.2020.120604
6. Mu X, Zhang M, Wei A, et al. Doxorubicin and PD-L1 siRNA co-delivery with stem cell membrane-coated polydopamine nanoparticles for the targeted chemoimmunotherapy of PCa bone metastases. *Nanoscale*. 2021;13(19):8998–9008. doi:10.1039/d0nr08024a
7. Bartlett JJ, Trivedi PC, Pulinilkunnil T. Autophagic dysregulation in doxorubicin cardiomyopathy. *J Mol Cell Cardiol*. 2017;104:1–8.
8. Wang T, Wang D, Yu H, et al. A cancer vaccine-mediated postoperative immunotherapy for recurrent and metastatic tumors. *Nat Commun*. 2018;9(1):1532. doi:10.1038/s41467-018-03915-4
9. Romine KA, MacPherson K, Cho HJ, et al. BET inhibitors rescue anti-PD1 resistance by enhancing TCF7 accessibility in leukemia-derived terminally exhausted $CD8^+$ T cells. *Leukemia*. 2023;37(3):580–592.
10. Tian Y, Wang X, Zhao S, et al. JQ1-loaded polydopamine nanoplatform inhibits c-MYC/Programmed Cell Death Ligand 1 to enhance photothermal therapy for triple-negative breast cancer. *ACS Appl Mater Interfaces*. 2019;11(50):46626–46636. doi:10.1021/acsami.9b18730
11. Gilan O, Rioja I, Knezevic K, et al. Selective targeting of BD1 and BD2 of the BET proteins in cancer and immunoinflammation. *Science*. 2020;368(6489):387–394. doi:10.1126/science.aaz8455
12. Ahmed NS, Gatchalian J, Ho J, et al. BRD9 regulates interferon-stimulated genes during macrophage activation via cooperation with BET protein BRD4. *Proc Natl Acad Sci U S A*. 2022;119(1):e2110812119. doi:10.1073/pnas.2110812119
13. Sun F, Zhu Q, Li T, et al. Regulating glucose metabolism with prodrug nanoparticles for promoting photoimmunotherapy of pancreatic cancer. *Adv Sci*. 2021;8(4):2002746. doi:10.1002/advs.202002746
14. Lai X, Stiff A, Duggan M, et al. Modeling combination therapy for breast cancer with BET and immune checkpoint inhibitors. *Proc Natl Acad Sci U S A*. 2018;115(21):5534–5539. doi:10.1073/pnas.1721559115
15. Wang H, Tang Y, Fang Y, et al. Reprogramming tumor immune microenvironment (TIME) and metabolism via biomimetic targeting co-delivery of Shikonin/JQ1. *Nano Lett*. 2019;19(5):2935–2944. doi:10.1021/acs.nanolett.9b00021

16. Elamin G, Aljoundi A, Soliman MES. Co-binding of JQ1 and venetoclax exhibited synergetic inhibitory effect for cancer therapy; potential line of treatment for the waldenström macroglobulinemia lymphoma. *Chem Biodivers*. 2022;19(7):e202100845. doi:10.1002/cbdv.202100845
17. Liu D, Li K, Gong L, et al. Charge reversal yolk-shell liposome co-loaded JQ1 and doxorubicin with high drug loading and optimal ratio for synergistically enhanced tumor chemo-immunotherapy via blockade PD-L1. *Pathway. Int J Pharm*. 2023;635:122728. doi:10.1016/j.ijpharm.2023.122728
18. Gu J, Zhao G, Yu J, et al. Injectable pH-responsive hydrogel for combinatorial chemoimmunotherapy tailored to the tumor microenvironment. *J Nanobiotechnology*. 2022;20(1):372. doi:10.1186/s12951-022-01561-z
19. Zhao H, Song Q, Zheng C, et al. Implantable bioresponsive nanoarray enhances postsurgical immunotherapy by activating pyroptosis and remodeling tumor microenvironment. *Adv Funct Mater*. 2020;30(51):2005747.
20. Gupta S, Gupta PK, Dharanivasan G, et al. Current prospects and challenges of nanomedicine delivery in prostate cancer therapy. *Nanomedicine (Lond)*. 2017;12(23):2675–2692. doi:10.2217/nnm-2017-0236
21. Zhao J, Zhang C, Wang W, et al. Current progress of nanomedicine for prostate cancer diagnosis and treatment. *Biomed Pharmacother*. 2022;155:113714. doi:10.1016/j.biopha.2022.113714
22. Budker VG, Monahan SD, Subbotin VM. Loco-regional cancer drug therapy: present approaches and rapidly reversible hydrophobization (RRH) of therapeutic agents as the future direction. *Drug Discov Today*. 2014;19(12):1855–1870. doi:10.1016/j.drudis.2014.08.009
23. Muhamad N, Plengsuriyakarn T, Na-Bangchang K. Application of active targeting nanoparticle delivery system for chemotherapeutic drugs and traditional/herbal medicines in cancer therapy: a systematic review. *Int J Nanomedicine*. 2018;13:3921–3935. doi:10.2147/IJN.S165210
24. Wolfram J, Ferrari M. Clinical cancer nanomedicine. *Nano Today*. 2019;25:85–98. doi:10.1016/j.nantod.2019.02.005
25. Wang Z, Chen Y, Zhang H, et al. Mitochondria-targeting polydopamine nanocomposites as chemophotothermal therapeutics for cancer. *Bioconjug Chem*. 2018;29(7):2415–2425. doi:10.1021/acs.bioconjchem.8b00325
26. Wu K, Zhou Z, Liu T, et al. Co-delivery of curcumin and si-STAT3 with a bioinspired tumor homing for polydopamine nanoparticles for synergistic osteosarcoma therapy. *Cancer Nanotechnol*. 2023;14:66.
27. Ruppel SS, Liang J. Tunable properties of polydopamine nanoparticles and coated surfaces. *Langmuir*. 2022;38(16):5020–5029.
28. Iyer AK, Khaled G, Fang J, et al. Exploiting the enhanced permeability and retention effect for tumor targeting. *Drug Discov Today*. 2006;11(17–18):812–818. doi:10.1016/j.drudis.2006.07.005
29. Yu F, Tu Y, Luo S, et al. Dual-drug backboned polyprodrug with a predefined drug combination for synergistic chemotherapy. *Nano Lett*. 2021;21(5):2216–2223. doi:10.1021/acs.nanolett.0c05028
30. Feng B, Hou B, Xu Z, et al. Self-amplified drug delivery with light-inducible nanocargoes to enhance cancer immunotherapy. *Adv Mater*. 2019;31(40):e1902960. doi:10.1002/adma.201902960
31. Zhang M, Zhang F, Liu T, et al. Polydopamine nanoparticles camouflaged by stem cell membranes for synergistic chemo-photothermal therapy of malignant bone tumors. *Int J Nanomedicine*. 2020;15:10183–10197. doi:10.2147/IJN.S282931